IEEE Access
Multidisciplinary | Rapid Review | Open Access Journal

Received December 13, 2018, accepted March 22, 2019, date of publication March 28, 2019, date of current version April 11, 2019.

Digital Object Identifier 10.1109/ACCESS.2019.2907659

Preparation, Characterization and Application of Ultrathick True Zero-Order KDP Crystal Waveplates

HONGKAI REN[1,2], ZHENGPING WANG[1,2], FANG WANG[3], FUQUAN LI[3], XUN SUN[1,2], AND XINGUANG XU[1,2]

[1]State Key Laboratory of Crystal Materials, Shandong University, Jinan 250100, China
[2]Key Laboratory of Functional Crystal Materials and Device, Ministry of Education, Shandong University, Jinan 250100, China
[3]Research Center of Laser Fusion, China Academy of Engineering Physics, Mianyang 621900, China

Corresponding author: Zhengping Wang (zpwang@sdu.edu.cn)

This work was supported by the Shandong Province Natural Science Foundation of China under Grant ZR2017MF031.

ABSTRACT In crystal space, the birefringence varies continuously with respect to the propagating direction of the light wave. By utilizing this property, we design and fabricate a series of ultrathick true zero-order (TZ) waveplates based on KH_2PO_4 crystals with different orientations for the first time. When the cutting angle θ is 5°, the thickness d of the 1,064-nm TZ half-wave plate (HWP) is 2.0 mm, which is 33 times larger than that of the traditional quartz TZ device (∼0.06 mm). At a temperature of 30 ° C, its extinction ratio for the Nd:YAG pulse laser reaches 1,970:1. When the temperature increases to 80 ° C, the extinction ratio remains above 1,000:1. When the extinction ratio decreases to 200:1, the angular acceptance bandwidth and wavelength acceptance bandwidth are determined to be 0.3° and 45 nm, respectively. With the ultrathick TZ HWP and a quarter-wave plate (QWP), efficient type-II frequency doubling and electro-optic Q-switching, respectively, are achieved. As a famous optical crystal, KDP has been popularly used as a frequency converter, a laser Q-switcher, an electro-optic modulator, and a solid-state light valve display. This paper disclosure a new application of this traditional material, i.e. large size, high mechanical strength, low-cost, and high-quality TZ crystal waveplates. Such components have wide application prospects in various optical and laser systems which need controlling the polarization of light.

INDEX TERMS True zero-order, crystal wave plate, KDP crystal, orientation, thickness, laser polarization.

I. INTRODUCTION

The waveplate, which is also known as a phase retarder, is an important optical component that can change the light polarization state by utilizing the birefringence feature [1]–[5]. It is employed in various optical and laser apparatuses related to light polarization, such as photoelastic instruments, polarimeters, and electro-optic (E-O) Q-switched solid-state lasers [6], [7]. In general, there are three types of waveplates: multiple-order waveplates (MWPs), true zero-order waveplates (TZWPs), and compound zero-order waveplates (CZWPs), which are composed of more than two plates. Compared with the MWP (phase retardation $\Delta\phi > 2\pi$), zero-order waveplates ($\Delta\phi < 2\pi$), especially the TZWP, have many advantages, including a wide operating waveband, high temperature stability, and a large acceptance angle.

Many materials have been used to fabricate waveplates, including bulk crystals (such as quartz [8], [9], sapphire [10], magnesium fluoride [10], and mica [11]), polymers [5], [12], liquid crystals [13], [14], two-dimensional layered materials [15], and plasmonic metasurfaces [16]. Among them, bulk crystals are the most mature and most widely used materials. Nevertheless, the conventional processing style, i.e., cutting along the principal axes, limits the thickness of the TZWP component to 0.01–0.1 mm. This makes the processing and application of centimeter-aperture crystal TZWPs very difficult. As a substitute, in many large-aperture optical systems, such as ultrahigh-power lasers, high-resolution inspection instruments, and astronomical observation equipment, quartz or sapphire MWPs are used as phase retarders or polarization-adjusting elements. However, the size of the crystal MWP

The associate editor coordinating the review of this manuscript and approving it for publication was Bora Onat.

is limited to 200 mm owing to the risk of fracture during polishing or application [17].

Compared with bulk crystals, polymer and liquid crystals are more suitable for the preparation of large TZWPs because of their ease of manufacturing and high homogeneity. Nevertheless, they both suffer from a relatively low laser damage threshold, and the transmission range of the polymer is mainly concentrated in the visible waveband. Thus, super-large, highly optical damage-resistant, wide-work waveband, true zero-order crystal waveplates are urgently needed for large-aperture, high-precision laser and optical systems. The most crucial problem in obtaining such waveplates is increasing the thickness of the TZWP.

Although in theory non-principal-axis processing is feasible for all types of crystals, it is seldom attempted for fabricating crystal waveplates. This phenomenon has possibly caused some of the practical problems with the traditional, widely used waveplate crystal materials, such as the high hardness (HM = 7) and growth stripe of quartz and the cleavage attribute of mica. In this study, we design and fabricate a series of TZWPs (1–10 mm in size) with non-principal-axis-processed KH_2PO_4 (KDP) crystals. The performance is satisfactory, and typical applications, such as extinction, type-II frequency doubling, and add-voltage style E-O Q-switching, are accomplished, which indicates an attractive application foreground. As the largest artificial crystal material in the world, the KDP-based TZWP exhibits excellent comprehensive properties, and its ability to be produced with a large size, at a large scale, and at low cost could help it find important, widespread applications in the future.

II. PREPARATION

A. THEORETICAL DESIGN

For an anisotropic optical crystal, the birefringence $\Delta n(\lambda,T)$ at a given wavelength λ and a given temperature T can be expressed as follows.

$$\Delta n(\lambda, T) = |n_o(\lambda, T) - n_e(\lambda, T)| \tag{1}$$

Here, $no(\lambda,T)$ and $ne(\lambda,T)$ are the ordinary and extraordinary refractive indices, respectively. For a familiar crystal waveplate that is processed along the principal optical axis, $no(\lambda,T)$ and $ne(\lambda,T)$are the refractive indices of the principal axes. The corresponding phase retardation $\Delta\phi$ is

$$\Delta\phi = \frac{2\pi}{\lambda} |n_o(\lambda, T) - n_e(\lambda, T)|\, d = \frac{2\pi}{\lambda} \Delta n(\lambda, T) d \tag{2}$$

where d is the thickness of the waveplate. For a half-wave plate (HWP) and a quarter-wave plate (QWP), the phase retardations can be written as

$$\Delta\phi_{HWP} = (2m + 1)\pi \tag{3}$$

$$\Delta\phi_{QWP} = \frac{(2m + 1)\pi}{2} \tag{4}$$

where m is an integer (the order of the waveplate). For quartz—a low-birefringence crystal-the thickness of true zero-order ($m = 0$) HWP at 1,064 nm is approximately 0.06 mm. To increase the robustness, the quartz crystal is often made into an MWP ($m > 0$) or CZWP, whose performances are significantly inferior to that of the TZWP. Obviously, the traditional processing style is unsuitable for a crystal with higher birefringence and a thinner TZWP. A special off-axis design can make the fabrication of the TZWP easier, as shown in Fig. 1(a). When a light beam passes through a uniaxial crystal at a small angle θ deviating from the optical axis, the birefringence $\Delta n'(\theta,\lambda,T)$ can be expressed as

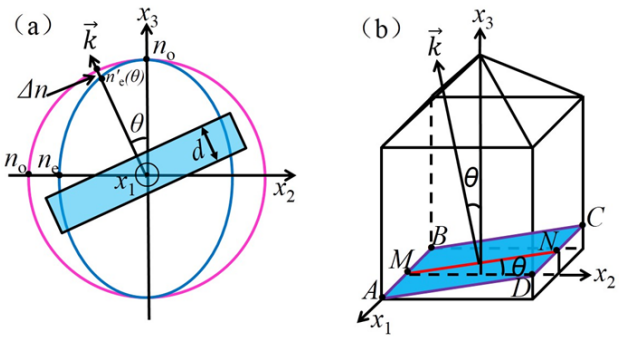

FIGURE 1. (a) Refractive index curved surfaces of a negative uniaxial crystal; (b) processing schematic of the KDP crystal waveplate.

$$\Delta n'(\theta, \lambda, T) = \left|n_o(\lambda, T) - n'_e(\theta, \lambda, T)\right| \tag{5}$$

where

$$n'_e(\theta, \lambda, T) = \frac{n_o(\lambda, T) n_e(\lambda, T)}{\sqrt{n_o^2(\lambda, T)\sin^2\theta + n_e^2(\lambda, T)\cos^2\theta}} \tag{6}$$

i.e., the refractive index of extraordinary light in this direction.

For a given phase retardation $\Delta\phi$, the geometrical thickness of a waveplate is

$$d(\theta, \lambda, T) = \frac{\Delta\phi\lambda}{2\pi\left|n_o(\lambda, T) - n'_e(\theta, \lambda, T)\right|} = \frac{\Delta\phi\lambda}{2\pi\,\Delta n'(\theta, \lambda, T)} \tag{7}$$

According to the refractive-index dispersion equations and thermo-optic coefficients of the crystal, the waveplate thickness d for different values of m, θ, λ, and T can be determined using Equations (3), (4), (6), and (7). The waveplate can be processed at different deviating angles θ; thus, its thickness can be selected from millimeter to centimeter order, and its mechanical strength can be increased drastically.

As a negative uniaxial crystal, KDP belongs to the point group $\bar{4}2m$. Its refractive indices can be expressed by two layer curved surfaces, as shown in Fig. 1(a). The corresponding cutting schematic of the KDP waveplate is presented in Fig. 1(b). The projection of the z-axis (i.e., the x_3-axis) acts as the waveplate "optic-axis" (MN), which is parallel to the edge (AD) or (BC) of the KDP waveplate ($ABCD$). A precise orientation, cutting, and polishing are needed for good optical retardation tolerances.

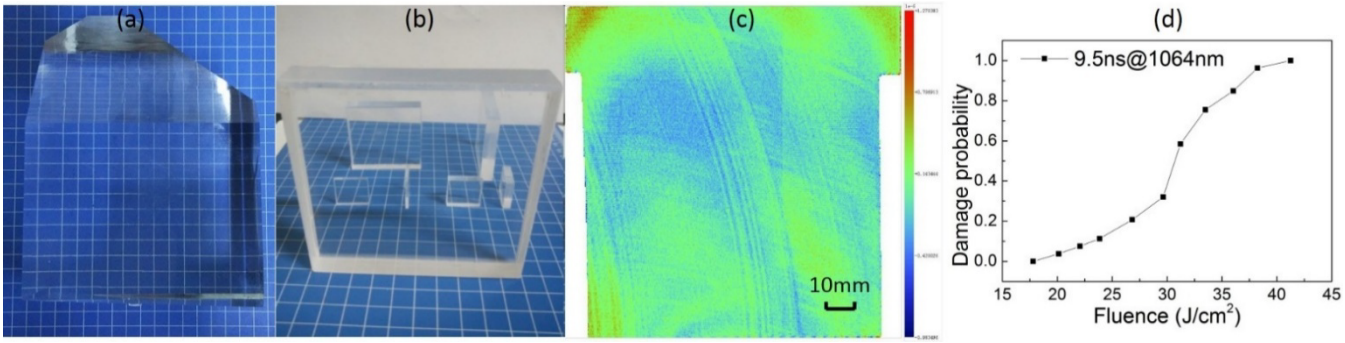

FIGURE 2. (a) As-grown KDP crystal with dimensions of 128 × 144 × 180 mm^3; (b) processed KDP waveplate samples with different sizes; (c) refractive-index inhomogeneity map of a large KDP waveplate; (d) measurement results for the optical damage.

TABLE 1. Thicknesses of KDP HWPs at 1,064 nm obtained from different references.

Sample No.	Angle θ (°)	Order m	Thickness d (mm)				
			Actual processing (295 – 298 K) this work	Zhu (293 K) [18]	Zernike (298 K) [19]	Ghosh (300 K) [20]	Kirby (306K) [21]
A2M0	2	0	12.41	12.27	12.45	12.42	12.43
A3M0	3	0	5.45	5.46	5.53	5.52	5.53
A4M0	4	0	3.05	3.07	3.12	3.11	3.11
A5M0	5	0	1.95	1.97	2.00	1.99	1.99
A5M1	5	1	5.97	5.90	5.99	5.98	5.98
A5M2	5	2	9.72	9.84	9.97	9.96	9.97

B. SAMPLE PREPARATION

1) CRYSTAL GROWTH

The KDP crystal was grown via the point-seed rapid growth method. The crystal growth solution was synthesized using extra pure-grade KDP and deionized water. Crystallization was performed in a 40-L Holden-type crystallizer with a temperature control accuracy of ±0.1 °C. The saturated temperature of the solution was determined to be 54.9 °C. The solution was filtered through a 0.05-μm filter and then overheated at 75 °C for more than 48 h. Then, the solution temperature decreased from 54.9 to 36.2 °C in 21 d. The as-grown crystals had sizes of 128 × 144 × 180mm^3 and no visible macroscopic defects, as shown in Fig. 2(a).

2) WAVE-PLATE PROCESSING

According to the theoretical model presented in Section 2.1, we produced KDP HWPs with different sizes, as shown in Fig. 2(b). The largest component reached 100 × 100 × 12 mm^3. It was chosen from the pyramid area, which avoided the sector boundaries successfully. For convenience, we standardized the sample aperture as 20 × 20 mm^2 in the characterization experiments presented in Section 3. For the target wavelength of 1,064 nm, the KDP HWPs were cut at angles θ of 2°, 3°, 4°, and 5° with a precision of ± 3′, and their transmission surfaces were polished but not coated. Table 1 presents the deviating angle θ, the order m, the corresponding processed thicknesses, and the theoretical calculated thicknesses based on different dispersion equations. The calculation results from all of the references are similar, and the absolute errors are smaller than ±0.1 mm. The dispersion equations of Zhu were formulated for a relatively low temperature of 293 K; thus, they lead to slightly smaller calculated results than the other equations. In total, we processed four pieces of the zero-order HWP and two pieces of the multiple-order HWP. In most cases, the actual thicknesses of the KDP waveplate samples were slightly smaller than the theoretical results; thus, their π or $\pi/2$ phase retardations may correspond to wavelengths slightly shorter than 1,064 nm.

3) QUALITY TESTING

To examine the quality of the KDP waveplate, we measured the refractive-index inhomogeneity and laser damage threshold. The results are shown in Figs. 2(c) and 2(d). The test samples were processed using diamond flying cutting technology. For the whole cross-section of the 100 × 100 × 12-mm^3 sample, the refractive-index inhomogeneity measured using a large-aperture interferometer (ϕ = 800 mm, VERY FIRE MST) was only 0.157 ppm (root-mean-square value). This corresponds to a refractive-index variation level of 10^{-7}, which can fully satisfy the application requirements of crystal waveplates. Taking the temperature property as an example, the refractive-index temperature coefficients of KDP crystal, $\partial n_o/\partial T$ and $\partial n_e/\partial T$, are at 10^{-5} order. So, comparing with the temperature, the intrinsic inhomogeneity is only a very minor factor that affects the phase variation, which can be neglected.

A $40 \times 40 \times 12$-mm^3 KDP waveplate was used to measure the laser damage property. The light source was a Nd:YAG laser with a wavelength of 1,064 nm and a pulse width of 9.5 ns. A lens with a focal length of 2 m was used to focus the laser beam onto the sample, and the focal spot diameter was 533.8 μm. Under the R-on-1 operating style, the lower and upper limits of the damage threshold were 17.1 and 20.6 J/cm^2, respectively. This indicates that the prepared KDP waveplate samples have good crystal quality and are suitable for the operating conditions of high-power lasers.

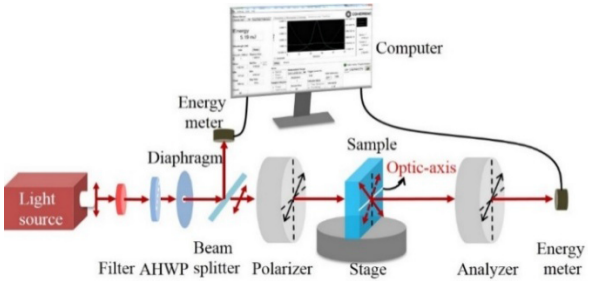

FIGURE 3. Experimental setup for characterizing the KDP HWPs.

III. CHARACTERIZATION

A. EXPERIMENTAL METHOD AND SETUP

The phase retardation of a waveplate depends on the temperature, light propagating direction (or incident angle), and wavelength. To characterize the properties of the KDP waveplate, the phase retardation must be examined with respect to the temperature, angle, and wavelength. In this study, we used the polarization interference method and the experimental setup shown in Fig. 3. The KDP sample was placed between the polarizer and the analyzer, whose polarization directions of transmission were parallel. There was an angle of 45° between the waveplate optic-axis and the polarization direction of the polarizer and analyzer. The transmission intensity of the system depends on the polarization state after the waveplate. The experimental conditions, including the temperature, angle, and wavelength, can affect the output polarization state of the waveplate by changing its phase retardation, which is reflected by the transmission intensity. Thus, the change of the phase retardation $\Delta\phi$ can be indirectly characterized by the parameter σ, where σ is the extinction ratio of the system, which is defined as E_i/E_o. E_o is the energy received after the analyzer, and E_i is the energy before the polarizer, which can be measured according to the reflected reference light, as shown in Fig. 3. As the reciprocal of the system transmittance, the extinction ratio σ is an important parameter for judging the quality of the HWP. A large extinction ratio represents high optical quality. According to the polarization optics theory, the system transmittance can be expressed as by Malus's law, i.e.

$$T_r = \frac{E_o}{E_i} = \cos^2 \frac{\Delta\phi}{2} \tag{8}$$

where $\Delta\phi$ is the phase retardation obtained using Equation (2). If the change of the incident angle is considered, $\Delta\phi$ has the following form:

$$\Delta\phi\,(\theta_0 + \theta_i, \lambda, T) = \frac{2\pi}{\lambda}\Delta n(\theta_0+\theta_i, \lambda, T)d\,(\theta_0+\theta_i, T) \tag{9}$$

where θ_0 is the π phase-retardation angle of the KDP HWP samples, and θ_i is the deviation angle relative to θ_0. In the ideal situation, when the waveplate reaches π phase retardation, the transmittance T_r is zero. This cannot be achieved in experiments, because of the optical homogeneity of the sample and the leakage of the testing system; thus, the measured transmittance can be written as

$$T_r\,(\theta_0 + \theta_i, \lambda, T) = T_{r0} + \cos^2 \frac{\Delta\phi\,(\theta_0+\theta_i, \lambda, T)}{2} \tag{10}$$

where T_{r0} is the residual transmittance at π phase retardation. According to Equations (9) and (10), we obtain the following.

$$\sigma\,(\theta_0 + \theta_i, \lambda, T) = \frac{1}{T_r} = \frac{1}{T_{r0} + \cos^2 \frac{\pi\Delta n(\theta_0+\theta_i,\lambda,T)d(\theta_0+\theta_i,T)}{\lambda}} \tag{11}$$

According to Equation (11), the measured data of the extinction ratio σ can be theoretically analyzed using the crystal parameters Δn and d or the experimental conditions $\theta_0 + \theta_i$, λ, and T.

In Fig. 3, two lasers are used successively as the light sources. One is a Q-switched Nd:YAG laser (Q-smart 850, Quantel Inc.) and is used to measure the temperature and angle sensitivity. It has a wavelength of 1,064 nm, a maximum output energy of 850 mJ, a line width of 0.7 cm^{-1}, a pulse width of 6 ns, a repetition rate of 10 Hz, and a beam divergence angle of 0.5 mrad. The other one is a tunable optical parametric oscillator (OPO) laser (Opolette HE 355 II, OPOTEK Inc.) that is used to measure the wavelength sensitivity. It has a wavelength tunable range of 410–2,400 nm, an adjusting step length of 1 nm, a pulse width of 4.5 ns, a spectral line width less than 7 cm^{-1}, a repetition rate of 20 Hz, and an output energy of $\sim$2 mJ around 1,064 nm. Its beam divergence is $<$10 mrad in the horizontal direction and $<$2 mrad in the vertical direction. In addition to the light sources, other components are used, including a filter, an achromatic HWP (AHWP), a diaphragm, a beam splitter, a polarizer, an analyzer, the KDP HWP sample, a precise multidimensional rotating stage, and an optical detecting system, as shown in Fig. 3. The filter is only used for the OPO laser to block the signal light located at the visible waveband; it is not used for the Nd:YAG laser. The AHWP is for polarization rotation, for which the operating waveband is 650–1,100 nm. The diaphragm (ϕ = 5 mm) is employed for beam shaping and also serves as a collimation screen for checking whether the light beam is perpendicular to the KDP sample by observing the position of the reflection spot. When the incident light arrives at the beam splitter, it is divided into the reference light E_r and the testing light E_i with an energy ratio of 1:4.2 and with very small deviation from 1,000 to 1,100 nm. Both the polarizer and the

analyzer are Glan–Taylor prisms (92% transmittance from 900 to 1,300 nm). The rotating stage can be used to adjust the spatial direction of the waveplate, and the temperature characteristic can be measured by depositing the waveplate into a temperature-controlled furnace. The optical detecting systems consist of two energy meters and a computer.

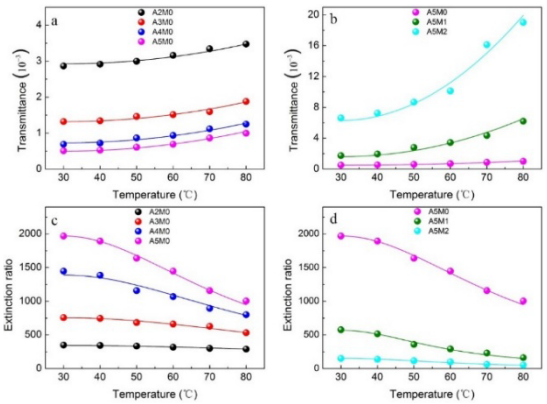

FIGURE 4. Changes of the transmittance and extinction ratio with respect to the temperature for different KDP HWP samples: (a, c) comparison of zero-order plates with different processing angles; (b, d) comparison of 0th, 1st, and 2nd-order plates with the same processing angle of 5°. The discrete points represent the experimental data, and the continuous lines represent the fitting curves.

B. TEMPERATURE SENSITIVITY

The temperature dependences of the transmittance and extinction ratio for the KDP HWP samples in Table 1 were experimentally measured in the range of 30-80 °C, as indicated by the discrete points in Fig. 4. The temperature adjusting interval was 10°C. At the lowest room temperature of 30 °C, all of the samples were adjusted to the π phase retardation; So, they exhibited their highest extinction ratios at this temperature. Then, the crystal temperature was slowly increased, and held 0.5 h at each experimental point before reading data. In this way, the temperature-field homogeneity of this experiment could be guaranteed.The transmittance results shown in Figs. 4(a) and 4(b) indicate that all of the zero-order HWPs have similar temperature sensitivity and that with the increase of the waveplate order, the temperature sensitivity increases rapidly.

As shown in Fig. 4(c), at the same temperature, the zero-order HWP with a larger processing angle always exhibited a higher extinction ratio. The samples A5M0 and A2M0 exhibited the highest and lowest extinction ratios, respectively. In theory, the extinction ratio is unrelated to the processing angle; however, the practical extinction ratio is related to the wafer thickness through the parameter T_{r0} in Equation (11). As shown in Table 1, among the zero-order HWPs, the sample with the smallest cutting angle has the largest thickness, which increases the inhomogeneity of the birefringence and yields a large T_{r0} under the optimum extinction conditions; thus, its extinction ratio is relatively low. In Fig. 4(d), the results for plates of different orders with the same processing angle of 5° are shown. At the same temperature, the zero-order sample A5M0 had a significantly higher extinction ratio than the other two samples, and the extinction ratio of the two-order sample A5M2 was the lowest. Similar to Fig. 4(c), this is attributed to the crystal thickness. At the same cutting angle, the zero-order sample had the smallest thickness and the lowest birefringence inhomogeneity; thus, its T_{r0} was the smallest, and its extinction ratio at π phase retardation was the highest.

At the lowest temperature of 30 °C, all of the samples were adjusted to the π phase retardation of incident light (1,064 nm); thus, they each exhibited their highest extinction ratio at this temperature. The sample A5M0 had the highest value of 1,970. With the increase of the temperature, the extinction ratios of all the samples decreased because of the deviation from π phase retardation, as shown in Fig. 4. Nevertheless, the extinction ratio of A5M0 remained above 1,000 when the temperature increased to 80 ° C.

The phase retardation $\Delta\phi$ at the temperature T can be expressed as

$$\Delta\phi\,(T) = \Delta\phi\,(T_0) + \Delta\phi^{'}\,(T) \tag{12}$$

where T_0 =30 °C, and $\Delta\phi(T_0) = (2m+1)\pi$. For 0^{th}, 1^{st}, and 2^{nd}-order HWPs, m = 0, 1, and 2, respectively. According to Equation (9)—omitting the minor term multiplied by the change of the refractive-index difference and the change of the crystal length—we obtain

$$\Delta\phi'\,(T) = (2m+1)\pi\left[\frac{1}{n_o - n_e'}\left(\frac{\partial n_o}{\partial T} - \frac{\partial n_e'}{\partial T}\right) + \alpha\right]\Delta T \tag{13}$$

where n_{o} and $n_{\text{e}}^{'}$ are the refractive indices of ordinary and extraordinary lights at 30 °, respectively, and $\partial n_{\text{o}}/\partial T$ and $\partial n_{\text{e}}^{'}/\partial T$ are their temperature coefficients, respectively. α is the thermal expansion coefficient along the transmission direction, which is taken as 4.2×10^{-5} [22]. $\Delta T = T - T_0$ represents the temperature variation amount. By substituting Equation (13) into Equations (10) and (11), the experimental data can be fitted with the parameter $\frac{1}{n_o - n_e'}\left(\frac{\partial n_o}{\partial T} - \frac{\partial n_e'}{\partial T}\right)$ as a variable. The fitting results for the transmittance and extinction ratio are shown as the solid curves in Fig. 4. The experimental data agree well with the fitting curves, indicating that the fitting results are reliable. The corresponding values of $\frac{1}{n_o - n_e'}\left(\frac{\partial n_o}{\partial T} - \frac{\partial n_e'}{\partial T}\right)$ are presented in Table 2, varying between 3.24 and 3.64 $\times\ 10^{-4}$/°. By substituting these values into Equation (13), the temperature-sensitivity parameter, $\Delta\phi'/\Delta T$, was obtained for each sample, as shown in Table 2. It expresses the change of the phase delay caused by the unit temperature and is basically proportional to the parameter $2m + 1$ ($m = 0, 1, 2$).

C. ANGLE SENSITIVITY

The variations of the transmittance and extinction ratio with respect to the external inclination angle θ' were measured for the six samples in Table 1, and the results are shown in Fig. 5.

TABLE 2. Temperature sensitivities of different KDP HWPS.

Sample	A2M0	A3M0	A4M0	A5M0	A5M1	A5M2
$\frac{1}{n_o-n_e}(\frac{\partial n_o}{\partial T}-\frac{\partial n_e'}{\partial T})$ (10^{-4}/°C)	3.64	3.28	3.58	3.32	3.34	3.24
$\Delta\phi'/\Delta T$ (mrad/°C)	1.28	1.16	1.26	1.17	3.54	5.75

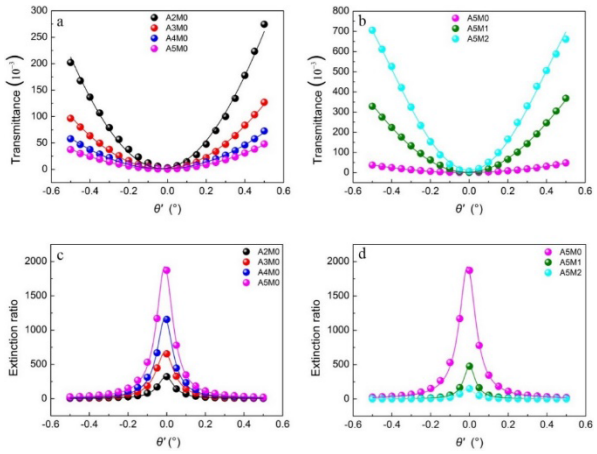

FIGURE 5. Changes of transmittance and extinction ratio with external inclining angle θ' for different KDP HWP samples: (a)(c) comparison of 0 order plates with different processing angles; (b)(d) comparison of 0, 1, 2 orders plates with the same processing angle of 5o. Discrete point: experimental data; continuous line: fitting curve.

According to the transmittance results of Figs. 5(a) and 5(b), among the zero-order HWPs, the angle sensitivity increases with the decrease of the cutting angle (θ_0), and among HWPs of different orders that have the same cutting angle, the angle sensitivity increases with the waveplate order. As a result, the sample A5M0 has the lowest angle sensitivity, and its angular acceptance bandwidth is 0.3° when the extinction ratio decreases to 200:1. For all of the samples, with the increase of the external inclination angle, the transmittance increased and the extinction ratio decreased because the phase differences gradually deviated from π.

The phase retardation $\Delta\phi$ at the crystal angle $\theta_0 + \theta_i$ can be expressed as

$$\Delta\phi\,(\theta_0+\theta_i) = \Delta\phi\,(\theta_0) + \Delta\phi'\,(\theta_0+\theta_i) \tag{14}$$

where $\theta_0 = 2°$, 3°, 4°, or 5° (i.e., the cutting angle of each sample), and $\Delta\phi(\theta_0) = (2m+1)\pi$. For 0^{th}, 1^{st}, and 2^{nd}-order HWPs, m = 0, 1, and 2, respectively. According to Equation (9)-omitting the minor term multiplied by the change of the refractive-index difference and the change of the transmission length-we obtain

$$\Delta\phi'\,(\theta_0+\theta_i) = (2m+1)\pi\left[\frac{1}{n_o-n_e'}\left(\frac{\partial n_o}{\partial\theta_i}-\frac{\partial n_e'}{\partial\theta_i}\right)+\frac{1}{d_0}\frac{\partial d}{\partial\theta_i}\right]\Delta\theta_i \tag{15}$$

where d_0 is the normal incidence thickness of the crystal plate, i.e., the transmission length corresponding to the π phase retardation.

The internal inclination angle θ_i and the external inclination angle θ' are related according to the refraction law, as follows.

$$n\sin\theta_i = \sin\theta' \tag{16}$$

Because the transmission direction is close to the optical axis z and both of the inclination angles are very small, $n \approx n_o$, $\sin\theta_i \approx \theta_i$, and $\sin\theta' \approx \theta'$. Thus, Equation (16) can be changed to $n_o\theta_i \approx \theta'$. Then, Equation (16) can be written as

$$\Delta\phi'\,(\theta_0,\theta\prime) = (2m+1)\pi\left[\frac{1}{n_o-n_e'}\left(\frac{\partial n_o}{\partial\theta\prime}-\frac{\partial n_e'}{\partial\theta\prime}\right)+\frac{1}{d_0}\frac{\partial d}{\partial\theta\prime}\right]\Delta\theta' \tag{17}$$

By substituting Equation (17) into Equations (10) and (11), the experimental data can be fitted with the parameter $\frac{1}{n_o-n_e'}(\frac{\partial n_o}{\partial\theta'}-\frac{\partial n_e'}{\partial\theta'})+\frac{1}{d_0}\frac{\partial d}{\partial\theta'}$ as a variable. The fitting results for the transmittance and extinction ratio are shown as the solid curves in Fig. 5. The experimental data agree well with the fitting curves, indicating that the fitting results are reliable. The corresponding fitting values of $\frac{1}{n_o-n_e'}(\frac{\partial n_o}{\partial\theta'}-\frac{\partial n_e'}{\partial\theta'})+\frac{1}{d_0}\frac{\partial d}{\partial\theta'}$ are presented in Table 3. By substituting these values into Equation (17), the angle-sensitivity parameter, $\Delta\phi'/\Delta\theta'$, was obtained for each sample, as shown in Table 3. It expresses the phase change caused by the unit external inclination angle, and its relative magnitude for each sample is consistent with the foregoing analyses regarding Figs. 5(a) and 5(b). If the internal inclination angle is of concern, the parameter $\Delta\phi'/\Delta\phi_i$ can be obtained by amplifying $\Delta\phi'/\Delta\theta'$ by a factor of 1.49 (n_o).

TABLE 3. Angle sensitivities of different KDP HWPs fitted by experimental data.

Sample	A2M0	A3M0	A4M0	A5M0	A5M1	A5M2
$\frac{1}{n_o-n_e}(\frac{\partial n_o}{\partial\theta'}-\frac{\partial n_e'}{\partial\theta'})+\frac{1}{d_0}\frac{\partial d}{\partial\theta'}$ (/°)	0.689	0.429	0.370	0.281	0.267	0.255
$\Delta\phi'/\Delta\theta'$ (rad/°)	2.16	1.35	1.16	0.88	2.52	4.01

In addition to the fitting using the experimental data, the angle-sensitivity parameter can be directly calculated from the crystal refractive indices. When the light deviates from the normal incident angle,

$$d = d_0/\cos\theta_i \tag{18}$$

Considering Equations (6) and (18) and $\partial n_o/\partial\theta_i = 0$, we obtain, (19), as shown at the bottom of the next page.

Fig. 5 indicates that $|\theta'| < 0.5°$, i.e., $|\theta_i| < 0.33°$, and $\sin\theta_i/\cos^2\theta_i < 0.006$. On the right-hand side of Equation (19), the first term is significantly larger than the second term; thus, in the following calculation, we omit the $\sin\theta_i/\cos^2\theta_i$

TABLE 4. Angle sensitivities of different KDP HWPs calculated from refractive indexes.

Sample	A2M0	A3M0	A4M0	A5M0	A5M1	A5M2
$\frac{1}{n_o-n_e'}(\frac{\partial n_o}{\partial\theta'}-\frac{\partial n_e'}{\partial\theta'})+\frac{1}{d_0}\frac{\partial d}{\partial\theta'}$ (/°)	0.669	0.445	0.334	0.267	0.267	0.267
$\Delta\phi'/\Delta\theta'$ (rad/°)	2.10	1.40	1.05	0.838	2.514	4.19

term. For each sample, by substituting n_o, n_e, $n_e'(\theta_0)$, and θ_0 into the first term on the right-hand side of Equation (19), we can obtain the approximate value of $\frac{1}{n_o-n_e'}(\frac{\partial n_o}{\partial\theta_i}-\frac{\partial n_e'}{\partial\theta_i})+\frac{1}{d_0}\frac{\partial d}{\partial\theta_i}$, which is converted into $\frac{1}{n_o-n_e'}(\frac{\partial n_o}{\partial\theta'}-\frac{\partial n_e'}{\partial\theta'})+\frac{1}{d_0}\frac{\partial d}{\partial\theta'}$ by dividing it by a factor of 1.49 (n_o). The results obtained from Equation (19) are in radians, and we converted them into degrees for comparison with Table 3, as shown in Table 4. By substituting $\frac{1}{n_o-n_e'}(\frac{\partial n_o}{\partial\theta'}-\frac{\partial n_e'}{\partial\theta'})+\frac{1}{d_0}\frac{\partial d}{\partial\theta'}$ into Equation (17), the values of $\Delta\phi'/\Delta\theta'$ were obtained, and shown in Table 4. The data in Table 4 are very close to the corresponding values in Table 3, indicating the reliability of our experiments and calculations.

For each KDP waveplate, there are two independent angle rotating styles: one is in the $\boldsymbol{x_2x_3}$ plane, and the other is in the $\boldsymbol{x_1k}$ plane, where $\boldsymbol{x_1}$, $\boldsymbol{x_2}$, and$\boldsymbol{x_3}$ are the crystal principal axes, and $\boldsymbol{k}$ is the vector direction of the waveplate, as shown in Fig. 1. The first rotating style is the variation of θ, which has been discussed above. By experiments and preliminary theoretical analysis, we confirm that the second rotating style is very insensitive to the angle variation; i.e., its angle sensitivity is significantly smaller than that of the first rotating style. Considering the second rotating style has very little effect on the practical application of waveplate, here we do not discuss it further.

D. WAVELENGTH SENSITIVITY

Using the OPO laser introduced in the fourth part of this paper, we examined the wavelength sensitivity for the KDP HWP samples in Table 1, with an adjusting interval of 5 nm. The experimental results are presented in Fig. 6. As shown in Figs. 6(a) and 6(b), the zero-order HWPs exhibited similar wavelength sensitivities, and the wavelength sensitivity increased rapidly with the increase of the waveplate order. Among the samples in Table 1, A5M0 has the maximum extinction ratio and its wavelength acceptance bandwidth is 45 nm when the extinction ratio decreases to 200:1. The maximum extinction ratio of each sample is determined by the parameter T_{r0}, which is associated with the thickness and

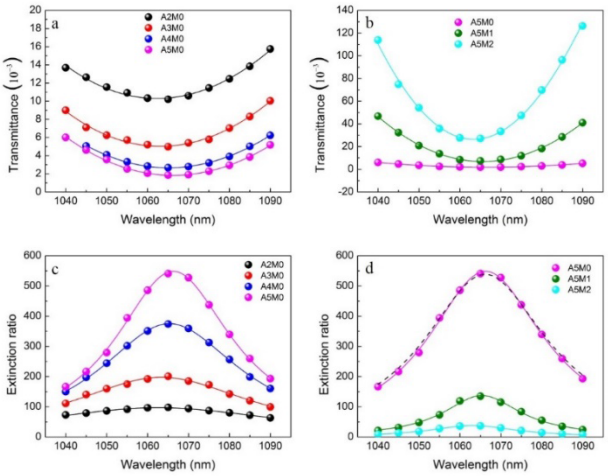

FIGURE 6. Changes of the transmittance and extinction ratio with respect to the wavelength for different KDP HWP samples: (a, c) comparison of zero-order plates with different processing angles; (b, d) comparison of 0th, 1st, and 2nd-order plates with the same processing angle of 5°. The discrete points represent the experimental data, and the continuous solid lines represent the fitting curves from the experimental points. The dashed lines represent the curve calculated from the Sellmeier equations for the KDP crystal.

homogeneity, as discussed in Section 3.2. Compared with the results in Figs. 4 and 5, the maximum extinction ratio of each sample in Fig. 6 is significantly lower. This is attributed to the change of the light source, as the monochromaticity and beam quality of the OPO laser were inferior to those of the Nd:YAG laser. In this experiment, all of the samples had a larger T_{r0}.

Because the wavelength of π phase retardation for all samples was pre-adjusted to 1,065 nm, we have

$$\Delta\phi\,(\lambda_0)=\frac{2\pi}{\lambda_0}\Delta n(\lambda_0)d=(2\mathrm{m}+1)\pi \tag{20}$$

where λ_0 = 1,065 nm. For 0^{th}, 1^{st}, and 2^{nd}-order HWPs, m = 0, 1, and 2, respectively. The phase retardation $\Delta\phi$ at the new wavelength λ can be expressed as

$$\Delta\phi\,(\lambda)=\Delta\phi\,(\lambda_0)+\Delta\phi'\,(\lambda) \tag{21}$$

Assuming that $\lambda=\lambda_0+\Delta\lambda$, from Equation (9), we obtain

$$\Delta\phi\,(\lambda)=\frac{2\pi}{\lambda_0+\Delta\lambda}\Delta n(\lambda_0+\Delta\lambda)d \tag{22}$$

According to the first-order Taylor series expansion of $(\lambda_0\Delta\lambda)^{-1}$, $\Delta n(\lambda_0+\Delta\lambda)=\Delta n(\lambda_0)+(\Delta n_o-\Delta n_e')$-omitting the minor term multiplied by $(\Delta n_o-\Delta n_e')$ and $\Delta\lambda$-we obtain

$$\Delta\phi'\,(\lambda)=(2m+1)\pi[\frac{1}{n_o-n_e'}(\frac{\partial n_o}{\partial\lambda}-\frac{\partial n_e'}{\partial\lambda})-\frac{1}{\lambda_0}]\Delta\lambda \tag{23}$$

$$\frac{1}{n_o-n_e'}(\frac{\partial n_o}{\partial\theta_i}-\frac{\partial n_e'}{\partial\theta_i})+\frac{1}{d_0}\frac{\partial d}{\partial\theta_i}=\frac{1}{2}n_on_e(\frac{n_o^2-n_e^2}{n_o-n_e'})\frac{\sin[2(\theta_0+\theta_i)]}{[n_o^2\sin^2(\theta_0+\theta_i)+n_e^2\cos^2(\theta_0+\theta_i)]^{1.5}}+\frac{\sin\theta_i}{\cos^2\theta_i} \tag{19}$$

TABLE 5. Wavelength sensitivities of different KDP HWPs fitted by experimental data.

Sample	A2M0	A3M0	A4M0	A5M0	A5M1	A5M2
$\frac{1}{n_o-n_e'}(\frac{\partial n_o}{\partial\lambda}-\frac{\partial n_e'}{\partial\lambda})$ (10^{-4}/nm)	-7.67	-7.30	-6.15	-6.25	-6.32	-6.36
$\Delta\phi'/\Delta\lambda$ (mrad/nm)	-5.36	-5.25	-4.89	-4.92	-14.82	-24.77

where n_o and n_e' are the refractive indices of ordinary and extraordinary lights at λ_0 (1,065 nm), respectively, and $\partial n_o/\partial\lambda$ and $\partial n_e'/\partial\lambda$ are their dispersion coefficients, respectively. By substituting Equation (23) into Equations (10) and (11), the experimental data can be fitted with the parameter $\frac{1}{n_o-n_e'}(\frac{\partial n_o}{\partial\lambda}-\frac{\partial n_e'}{\partial\lambda})$ as a variable. The fitting results for the transmittance and extinction ratio are shown as the continuous solid curves in Fig. 6, which agree well with the experimental data. The corresponding values of $\frac{1}{n_o-n_e'}(\frac{\partial n_o}{\partial\lambda}-\frac{\partial n_e'}{\partial\lambda})$ are listed in Table 5, varying between -1.71 and -1.55×10^{-3}/nm. By substituting these values into Equation (23), the wavelength-sensitivity parameter, $\Delta\phi'/\Delta\lambda$, can be obtained for each sample, as shown in Table 5. It represents the change of the phase delay caused by the unit wavelength and is basically proportional to the parameter $2m+1$ ($m=0, 1, 2$).

Similar with the angle sensitivity parameter, the wavelength sensitivity parameter can also be directly calculated from the refractive index dispersions of KDP crystal. From different Sellmeier equations [19], [20], [23], the same $\frac{1}{n_o-n_e'}(\frac{\partial n_o}{\partial\lambda}-\frac{\partial n_e'}{\partial\lambda})$ value of -5.52×10^{-4}/nm is obtained, which is close to the fitted data in table 5. With the sample A5M0 as example, we calculated its extinction ratio dispersion curve using this value, as the dashed line demonstrated in Fig. 6(d). It can be seen that the calculated curve is basically accordant with the experimental data and their fitting curve, which proves the reliability of our experimental results again.

IV. APPLICATION

A. TYPE-II FREQUENCY DOUBLING

The linear polarization of a commercial laser is always along the vertical or horizontal direction. For satisfying the type-II frequency-doubling phase-matching condition, there are two methods: in the first, the frequency-doubling crystal rotates 45° around the wave vector direction $\boldsymbol{k}$, and in the second, the polarization of the fundamental light rotates 45° around $\boldsymbol{k}$ with an HWP. In Fig. 7, we compare the experimental results of these two methods. The fundamental light source is a dye mode-locked 1,064-nm Nd:YAG laser (PY61C-10, Continuum Inc., USA) with a pulse width of 40 ps and a pulse repetition rate of 10 Hz. The type-II frequency-doubling crystal is a KDP crystal that is processed along the (59°, 0°) direction and has dimensions of $20\times20\times10$ mm^3. A $\phi=4$ mm diaphragm is set before the frequency-doubling crystal to improve the beam quality of the incident light.

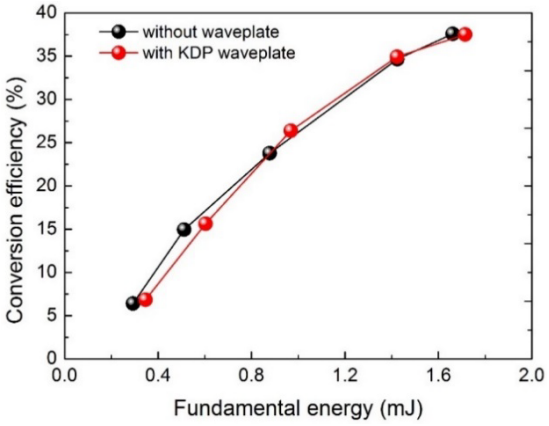

FIGURE 7. Type-II frequency-doubling conversion efficiency with respect to the fundamental energy for the two methods.

The sample HWP-A5M0 is used for the second method, and its surface reflection losses are shown in Fig. 7. The conversion efficiencies of the two methods are basically identical throughout the entire fundamental energy scope, which confirms that the KDP TZWP can be practically applied to the polarization rotation of type-II frequency doubling.

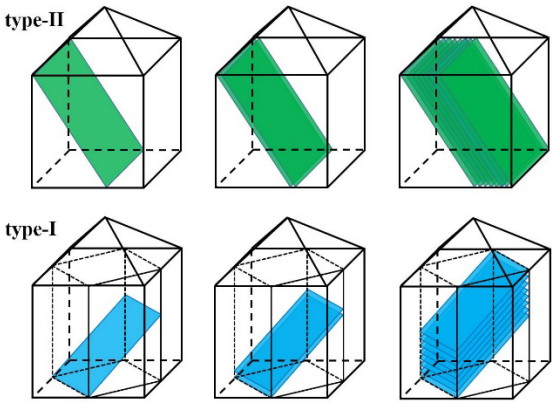

FIGURE 8. Processing diagrams of large aperture KDP frequency doubling devices.

From the viewpoint of preparing large-aperture nonlinear optical (NLO) components, type-II frequency-doubling devices are significantly different from the type-I frequency doubler. Taking the 1,064-nm Nd:YAG laser as an example, the cutting angle is (59°, 0°) for the type-II KDP frequency doubler and (41°, 45°) for the type-I KDP frequency doubler, as shown in Fig. 8. According to the principles of stereoscopic geometry, it can be calculated that for the same aperture frequency-doubling components of 420 cm × 420 cm, the blank volume of the KDP crystal required for type-II cutting is approximately 420 cm × 210 cm × 360 cm, while that required for type-I cutting is approximately 500 cm × 500 cm × 300 cm. Thus, the KDP crystal blank volume required for type-I cutting is far larger than that required for type-II cutting, which greatly increases the difficulties of crystal growth, processing, shaping, and batch supply, as well as the difficulty of reaching the standards for the optical

uniformity and the laser damage threshold. In addition, with regard to the NLO technology, the angular acceptance width of type-II frequency conversion is larger than that for type-I. Therefore, the type-II frequency-doubling scheme has great research significance and application value.

For type-II frequency doubling of a small-aperture laser, although the first method (rotating the NLO crystal) appears convenient, its output with 45° polarization inclination often introduces issues for subsequent applications. For a large-aperture laser, the shortcomings of the first method are more obvious. It brings great inconvenience to light-path adjustment and beam marshaling, and it causes changes in the beam diameter and output energy. In contrast, the second method is relatively convenient and does not reduce the beam diameter when the output energy is optimized. In addition, the KDP blank used to fabricate large-aperture waveplates is not difficult to obtain. The cutting direction deviates from the z-axis by only a few degrees (Fig. 1) and basically coincides with the growth direction of the as-grown boule; thus, it is easy to cut out large waveplate devices with a high laser damage threshold.

In summary, type-II frequency doubling has advantages over type-I frequency doubling, such as easier device preparation and a larger angular acceptance width. For type-II frequency doubling, the HWP method has an adjustment advantage over the NLO crystal rotating method. Thus, the KDP TZWP is promising for important applications in various large-aperture, high-power laser systems.

B. ELECTRO-OPTIC Q-SWITCHING

E-O Q-switching is an important technology for achieving high-energy lasers. For add-voltage-style E-O Q-switching, the QWP is a necessary optical component for adjusting the low Q state, i.e., the ''close-door'' state, when voltage is not added to the Q-switcher. This operation style is favorable for short pulses and a high peak power of the laser output. Quartz, mica, or sapphire QWPs are typically used in such equipment. In this study, high-performance add-voltage E-O Q-switching was successfully realized using a zero-order KDP QWP.

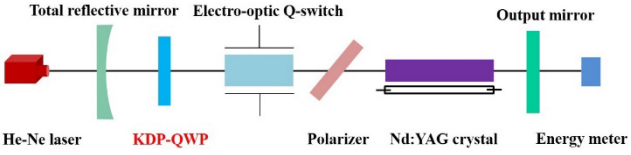

FIGURE 9. Experimental setup of add-voltage style E-O Q-switching.

The experimental setup is shown in Fig. 9. The length of the concave-flat laser resonator was approximately 100 cm. The left-end concave mirror was a total reflective mirror at 1,064 nm with a curvature of 3 m. The right-end flat mirror was a partially reflective mirror with a transmittance of 80% at 1,064 nm and served as the output mirror. A He-Ne laser was used as the collimated light source. The laser medium was a Nd:YAG rod ϕ 6.3 mm × 130 mm in size, which was pumped by a xenon lamp whose work repetition rate was 1 Hz. The polarizer was set at the Brewster angle for selecting the linear polarization direction of the output laser. The E-O Q-switch was made of a high-quality $La_3Ga_5SiO_{14}$ (langasite) crystal. The KDP-QWP, which was denoted as QWP-A2M0, was a zero-order waveplate that was processed along $\theta = 2°$ and was 6.16 mm thick.

The Q-switching operation principle can be simply described as follows. A polarizer and a QWP are deposited in the laser resonator simultaneously. When the intracavity laser propagates leftward and rightward two times, the Q-switch with zero applied voltage adds no phase retardation, but the QWP adds π phase retardation; thus, the laser is blocked by the polarizer because its polarization has rotated 90° . This corresponds to the high-loss (low-Q) state of the resonator. When a quarter-wave voltage is applied to the Q-switch, it introduces additional π phase retardation for the double-passed laser; thus, the laser can pass through the polarizer and then obtain constant amplification and output, because the total phase retardation is 2π and its polarization state has not changed. This corresponds to the low-loss (high-Q) state of the resonator.

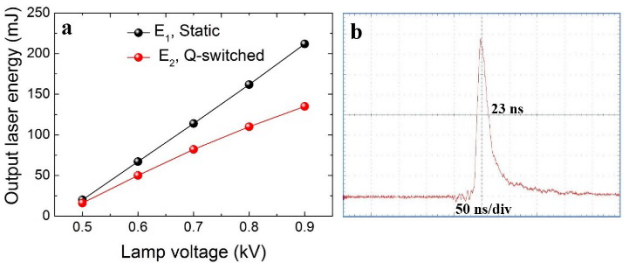

FIGURE 10. E-O Q-switching characteristics. (a) output energy; (b) single pulse waveform.

The experimental results are shown in Fig. 10. Here the static laser output was measured when the KDP-QWP was removed out of laser cavity, at the same time no voltage was added on the Q-switch. When the lamp voltage is 900 V, the maximum static output energy E_1 is 212 mJ. At the same lamp voltage, the maximum dynamic energy E_2 reaches 135 mJ, corresponding to a high dynamic–static ratio of $E_2/E_1 = 64\%$. At low-voltage points, the dynamic–static ratio can exceed 80%. Throughout the operation process, short and clean laser pulses are observed, and no damage is found on QWP-A2M0. The waveform of the single laser pulse at a lamp voltage of 900 V is presented in Fig. 10(b), with a pulse width of 23 ns. The results indicate the excellent practicability of the KDP TZWP.

V. CONCLUSIONS

The word ''data'' is plural, not singular.

For the first time, Non-principal-axis-processed ultrathick KDP TZWPs were designed, investigated, and applied. Excellent phase-retardation characteristics were observed. Taking the sample HWP-A5M0 as an example, its temperature, angle, and wavelength sensitivities were determined to be 1.17 mrad/°C, 0.88 rad/°, and -4.92 mrad/nm, respectively. Its highest extinction ratio was $\sim 2 \times 10^3$ for a 1,064-nm pulse laser. Using the KDP TZWPs, we efficiently realized two

representative applications: polarization rotation for type-II frequency doubling and add-voltage-style E-O Q-switching. The rich advantages of the KDP TZWPs, such as their large size, robustness, low cost, flexible design, easy processing, low temperature, and wavelength sensitivity, may help them find extensive applications in various optical and laser systems. Curriculum Vitae.

REFERENCES

[1] S. Shichi, M. Fujii, and S. Hayashi, "Ultraviolet true zero-order wave plate made of birefringent porous silica," *Opt. Lett.*, vol. 36, no. 19, pp. 3951–3953, Oct. 2011.
[2] C. Wu, H. Li, X. Yu, F. Li, H. Chen, and C. T. Chan, "Metallic helix array as a broadband wave plate," *Phys. Rev. Lett.*, vol. 107, no. 17, Oct. 2011, Art. no. 177401.
[3] Y. Gorodetski, E. Lombard, A. Drezet, C. Genet, and T. W. Ebbesen, "A perfect plasmonic quarter-wave plate," *Appl. Phys. Lett.*, vol. 101, no. 20, 2012, Art. no. 201103.
[4] M. J. Abuleil and I. Abdulhalim, "Tunable achromatic liquid crystal waveplates," *Opt. Lett.*, vol. 39, no. 19, pp. 5487–5490, Oct. 2014.
[5] J.-G. Lim, K. Kwak, and J.-K. Song, "Computation of refractive index and optical retardation in stretched polymer films," *Opt. Express*, vol. 25, no. 14, pp. 16409–16418, Jul. 2017.
[6] K. Liu *et al.*, "Pulse width adjustable Q-switched cavity dumped laser by rotating a quarter-wave plate and a pockels cell," *Opt. Lett.*, vol. 42, no. 13, pp. 2467–2470, Jul. 2017.
[7] H. Qi, Z. Wang, F. Yu, X. Sun, X. Xu, and X. Zhao, "Cascaded third-harmonic generation with one KDP crystal," *Opt. Lett.*, vol. 41, no. 24, pp. 5823–5826, Dec. 2016.
[8] N. N. Nagib, S. A. Khodier, and H. M. Sidki, "Retardation characteristics and birefringence of a multiple-order crystalline quartz plate," *Opt. Laser Technol.*, vol. 35, no. 2, pp. 99–103, 2003.
[9] A. Saha, K. Bhattacharya, and A. K. Chakraborty, "Achromatic quarter-wave plate using crystalline quartz," *Appl. Opt.*, vol. 51, no. 12, pp. 1976–1980, Apr. 2012.
[10] V. Chandrasekharan and H. Damany, "Birefringence of sapphire, magnesium fluoride, and quartz in the vacuum ultraviolet, and retardation plates," *Appl. Opt.*, vol. 7, no. 5, pp. 939–941, May 1968.
[11] S. Chu, R. Conti, P. Bucksbaum, and E. Commins, "Making mica retardation plates: A simple technique," *Appl. Opt.*, vol. 18, no. 8, pp. 1138–1139, Apr. 1979.
[12] H. J. Ryu, J. Hwang, J. Kim, and J.-H. Lee, "Dependence of the birefringence of polystyrene film on the stretching conditions," *Appl. Opt.*, vol. 57, no. 2, pp. 268–272, Jan. 2018.
[13] A. B. Golovin, S. V. Shiyanovskii, and O. D. Lavrentovich, "Fast switching dual-frequency liquid crystal optical retarder, driven by an amplitude and frequency modulated voltage," *Appl. Phys. Lett.*, vol. 83, no. 19, pp. 3864–3866, 2003.
[14] M. D. Lavrentovich, T. A. Sergan, and J. R. Kelly, "Switchable broadband achromatic half-wave plate with nematic liquid crystals," *Opt. Lett.*, vol. 29, no. 12, pp. 1411–1413, 2004.
[15] H. Yang *et al.*, "Optical waveplates based on birefringence of anisotropic two-dimensional layered materials," *ACS Photon.*, vol. 4, no. 12, pp. 3023–3030, 2017.
[16] F. Ding, Z. Wang, S. He, V. M. Shalaev, and A. V. Kildishev, "Broadband high-efficiency half-wave plate: A supercell-based plasmonic metasurface approach," *ACS Nano.*, vol. 9, no. 4, pp. 4111–4119, Mar. 2015.
[17] S. D. Jacobs, Y. Asahara, and T. Izumitani, "Optical glass wave plates," *Appl. Opt.*, vol. 21, no. 24, pp. 4526–4532, Dec. 1982.
[18] L. Zhu *et al.*, "Refractive indices in the whole transmission range of partially deuterated KDP crystals," *AIP Adv.*, vol. 3, no. 11, 2013, Art. no. 112114.
[19] F. Zernike, "Refractive indices of ammonium dihydrogen phosphate and potassium dihydrogen phosphate between 2000 Å and 1.5 μ," *J. Opt. Soc. Amer. A, Opt. Image Sci.*, vol. 54, no. 10, pp. 1215–1220, 1964.
[20] G. Ghosh and G. Bhar, "Temperature dispersion in ADP, KDP, and KD P for nonlinear devices," *IEEE J. Quantum Electron.*, vol. 18, no. 2, pp. 143–145, Feb. 1982.
[21] K. W. Kirby and L. G. DeShazer, "Refractive indices of 14 nonlinear crystals isomorphic to KH_2PO_4," *J. Opt. Soc. Amer. B, Opt. Phys.*, vol. 4, no. 7, pp. 1072–1078, 1987.
[22] W. R. Cook, Jr., "Thermal expansion of crystals with KH_2PO_4 structure," *J. Appl. Phys.*, vol. 38, no. 4, pp. 1637–1642, 1967.
[23] N. P. Barnes, D. J. Gettemy, and R. S. Adhav, "Variation of the refractive index with temperature and the tuning rate for KDP isomorphs," *J. Opt. Soc. Amer.*, vol. 72, no. 7, pp. 895–898, 1982.

HONGKAI REN received the B.S. degree in applied physics from the Hebei University of Science and Technology, in 2013. He is currently pursuing the Ph.D. degree with Shandong University with a focus on polarization and nonlinear optical materials related learning and research.

ZHENGPING WANG he received the bachelor's, master's, and Ph.D. degrees from Shandong University, in 1996, 1999, and 2002, respectively, where he is currently a Professor with the Institute of Crystal Materials. He has authored more than 300 scientific research papers (including more than 100 as the first or the corresponding authors), and 22 pieces of invention patents. His main research interests include laser and nonlinear optical materials.

FANG WANG received the B.S. degree from Tsinghua University and the M.S. degree from Graduate School, China Academy of Engineering Physics (CAEP), Mianyang, China, where she is currently an Associate Professor with the Research Center of Laser Fusion. Her recent work covers frequency conversion, beam control, and nonlinear propagation in high power laser systems.

FUQUAN LI received the M.S. degree from the University of Electronic Science and Technology of China, in 2002. In 2016, he became a Researcher dedicated to laser control technology with the Research Center of Laser Fusion, China Academy of Engineering Physics (CAEP), Mianyang, China. Since 2002, he has been with the CAEP.

XUN SUN received the bachelor's, master's, and Ph.D. degrees from Shandong University. He is currently a Professor with the Institute of Crystal Materials, Shandong University. He is mainly interested in functional crystal material preparation and performance, crystal growth kinetics, and large-size KDP/DKDP single crystal growth and related performance characterization.

XINGUANG XU was born in 1964. He received the bachelor's, master's, and Ph.D. degrees from Shandong University. He is currently a Professor with the Institute of Crystal Materials and an Academic Committee of the State Key Laboratory of Crystal Materials, Shandong University. He is also a Member of the ICF Expert Group of the Ministry of Education, China. He focuses on the research of crystal physics, crystal devices, nonlinear optics, and super-large crystal growth and processing.